analytical chemistry

Article

Cite This: *Anal. Chem.* 2019, 91, 14231−14238

pubs.acs.org/ac

In-Line Ultrasound-Enhanced Raman Spectroscopy Allows for Highly Sensitive Analysis with Improved Selectivity in Suspensions

Karin Wieland, Stefan Tauber, Christoph Gasser, Lukas A. Rettenbacher, Laurin Lux, Stefan Radel, and Bernhard Lendl*

Institute of Chemical Technologies and Analytics, Research Division Environmental, Process Analytics and Sensors, TU Wien, 1060 Vienna, Austria

Supporting Information

ABSTRACT: Raman spectroscopy is a nondestructive characterization method offering chemical-specific information. However, the cross-section of inelastically (Raman) scattered light is very low compared to elastically (Rayleigh) scattered light, resulting in weak signal intensities in Raman spectroscopy. Despite providing crucial information in off-line measurements, it usually is not sensitive enough for efficient, in-line process control in conjunction with low particle concentrations. To overcome this limitation, two custom-made 1.4404 stainless-steel prototype add-ons were developed for in-line Raman probes that enable ultrasound particle manipulation and thus concentration of particles in suspensions in the focus of the Raman excitation laser. Depending on size and density differences between particles and the carrier medium, particles are typically caught in the nodal planes of a quasi-standing wave field formed in an acoustic resonator in front of the sensor. Two arrangements were realized with regard to the propagation direction of the ultrasonic wave relative to the propagation direction of the laser. The parallel arrangement improved the limit of detection (LOD) by a factor of ≈30. In addition to increased sensitivity, the perpendicular arrangement offers increased selectivity: modifying the frequency of the ultrasonic wave field allows the liquid or solid phase to be moved into the focus of the Raman laser. The combination of in-line Raman spectroscopy with ultrasound particle manipulation holds promise to push the limits of conventional Raman spectroscopy, hence broadening its field of application to areas where previously Raman spectroscopy has not had sufficient sensitivity for accurate, in-line detection.

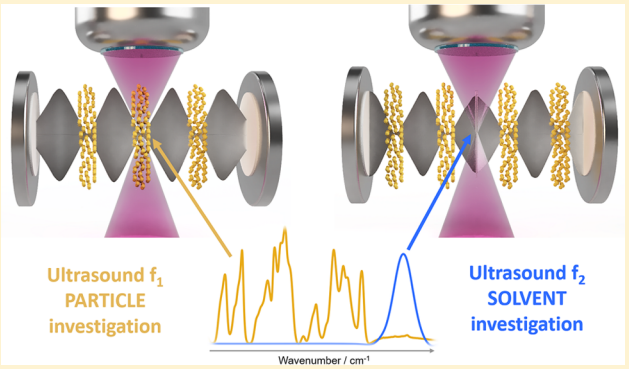

Raman spectroscopy is a valuable tool for direct, fast, nondestructive, and label-free investigation of gaseous, liquid, and solid samples.[1−5] Especially for process monitoring purposes, Raman offers the possibility of real-time reaction monitoring in aqueous environments by analyzing chemical fingerprints specific to the analyte of interest.[6−8] While Raman offers unique insights for process control, it suffers from low signal intensity due to its small cross-section. In-line probes for process monitoring are currently insufficiently sensitive to access small changes in the spectral fingerprint that might be crucial for the differentiation of two chemically similar components (e.g., polymorphs in crystallization processes) or for early detection of the formation of a specific analyte. Earlier detection of wanted or unwanted analytes in (bio)processes allows better adaption and optimization of these processes. Efficient process control is directly linked to improved production cycles, resulting in more efficient work load systems and hence more cost-efficient production. Koch et al. have performed highly sensitive in-line ultrasound-enhanced attenuated total reflection (ATR) mid-infrared spectroscopy in bioreactors by using ultrasonic standing wave fields to manipulate particles, pushing the analyte against the surface of the ATR element and thus into the evanescent field.[9] Combination of ultrasound particle manipulation (UPM) with Raman spectroscopy as a less water-sensitive method has also been shown to facilitate spectroscopy in aqueous suspensions while simultaneously allowing significantly higher signal intensities. In these experiments, a flow cell was used to investigate theophylline crystals or yeast cells or to perform surface-enhanced Raman spectroscopy (SERS).[10,11] Herein, we introduce a prototype add-on made of stainless steel for fiber-optic in-line Raman probes that allows UPM, hence enabling measurements with significantly lower limits of detection (LODs). Briefly, an acoustic resonator is built in front of the probe. Homogeneously distributed particles in a stirred suspension are either drawn into pressure or antipressure areas of the acoustic standing wave field depending on the material properties, such as particle size, density, and

Received: March 1, 2019
Accepted: October 15, 2019
Published: October 15, 2019

DOI: 10.1021/acs.analchem.9b01105
Anal. Chem. 2019, 91, 14231−14238

compressibility, of the particles and the surrounding medium and the ratios thereof. The design of an ultrasound add-on for in-line Raman probes furthers two main goals: (i) improve the sensitivity of in-line Raman probes for particle measurements and (ii) enhance selectivity of in-line Raman measurements of suspensions to selectively investigate either the solid or liquid phase of a two-component system. To this end, two different designs were realized: (a) arranging the ultrasonic wave parallel to the direction of laser propagation allows investigation of two model aqueous systems (starch and PMMA) that differ mainly in particle size. Improvements in the LOD by a factor of ≈30 were achieved, highlighting the potential of this technique to further extend the lower end of the accessible concentration range of conventional Raman spectroscopy. (b) Arranging the ultrasonic wave perpendicular to the direction of laser propagation not only offers improved sensitivity but also allows particles to be selectively moved into or out of the Raman laser focus by changing the frequency of the ultrasonic waves. Hence, detailed investigation of either the liquid phase or the solid phase is possible.

ULTRASONIC PARTICLE MANIPULATION

The combination of Raman spectroscopy with UPM was achieved by developing a prototype add-on to a Raman in-line probe that allows the formation of an ultrasound standing wave field and thus concentration of particles right in front of the Raman sensor. An acoustic resonator consisting of a transducer and a reflector was employed to generate the ultrasound standing wave field. Superposition of the incoming and reflected waves results in the formation of a quasi-standing wave field within the resonator. By placing this resonator in a suspension, particles are forced into the nodal or antinodal planes of the standing wave field mainly due to the primary axial radiation force F_z^{rad} acting on them. Considering a suspension with particles of radius r and a wavelength λ of the pressure wave propagating in the z-direction, the primary axial radiation force F_z^{rad} for particles with $r \ll \lambda$ can be described as[12]

$$F_z^{\mathrm{rad}} = 4\pi \times \Phi(\tilde{\kappa}, \tilde{\rho}) \times (kr)^3 \times E_{ac} \times \sin(2kz) \quad (1)$$

where the acoustic contrast factor $\Phi(\tilde{\kappa}, \tilde{\rho})$ is defined as[12]

$$\Phi(\tilde{\kappa}, \tilde{\rho}) = \frac{1}{3}\left(\frac{5\tilde{\rho} - 2}{2\tilde{\rho} + 1} - \tilde{\kappa}\right) \quad (2)$$

with density ratio $\tilde{\rho} = \rho_p/\rho_0$ of the particles ρ_p and the surrounding medium ρ_0 and compressibility ratio $\tilde{\kappa} = \kappa_p/\kappa_0 = \frac{1}{\rho_p c_p^2}/\frac{1}{\rho_0 c_0^2}$. Furthermore, F_z^{rad} is proportional to the acoustic energy factor E_{ac}, which describes the energy brought into the system as[12]

$$E_{ac} = \frac{p_a^2}{4\rho_0 c_0^2} \quad (3)$$

where p_a is the acoustic pressure amplitude, ρ_0 is the density of the medium, and c_0 is the speed of sound in the medium. The primary axial radiation force is predominantly affected by the radius of the particles ($F_z^{\mathrm{rad}} \sim r^3$). Due to this strong dependence, in this study, we focus on particles with narrow size distribution. This ensures uniform rearrangement of the particles in the quasi-standing acoustic wave field. Additional parameters such as the density and compressibility ratios of the particles and the medium also have an impact on F_z^{rad}, which, however, typically is comparatively low and, hence, insignificant compared to the particle size. Other, less intense, forces also affect the local particle arrangement within the nodal planes (see Figure 1a): the action of the transverse primary

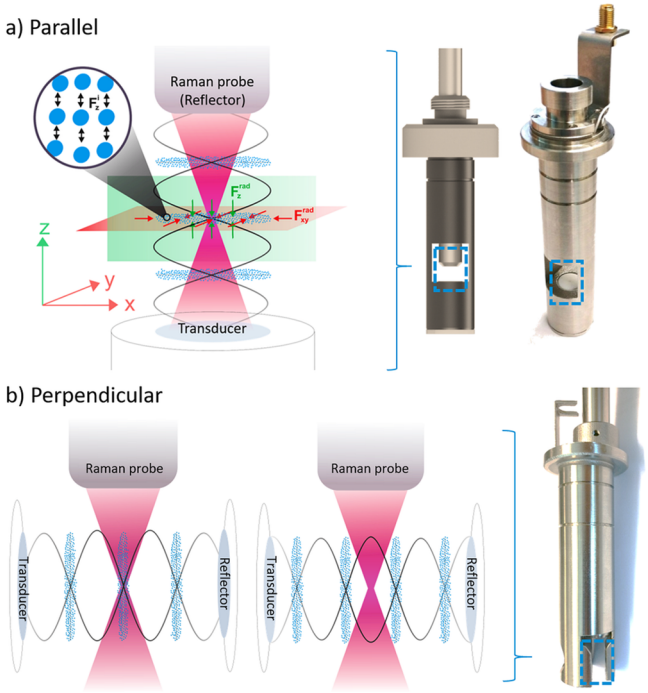

Figure 1. Two arrangements of the ultrasonic wave propagation direction with respect to the Raman excitation laser propagation direction: (a) in the parallel arrangement, particles are accumulated in the nodal planes of the standing wave in front of the probe, resulting in increased signal intensity. (b) In the perpendicular arrangement, the frequency of the ultrasonic wave can be shifted, allowing investigation of the solid (left) or liquid (right) phase of a suspension, thus resulting in increased selectivity as well as sensitivity.

radiation force F_{xy}^{rad} perpendicular to the sound propagation direction results from uneven amplitude contributions and is hence an effect of deviations from an ideal resonator. The secondary radiation force F_{xyz}^{i} describes the interaction between closely spaced particles in the nodal planes. Detailed descriptions of these forces are given elsewhere.[13−16]

EXPERIMENTAL SECTION

Ultrasonic Resonator. Prototype ultrasound add-ons to in-line Raman probes were fabricated out of 1.4404 stainless steel by selective laser melting. The dimensions of both prototypes were adapted to fit a D25 Ingold port. The 1 mm-thick piezoelectric ceramics (PZT, PI Ceramic GmbH, Germany) with printed silver electrodes were isolated from the aqueous suspension via an additional layer of Macor ceramics (Corning Inc., NY), forming the ultrasound transducer. Macor is a machinable glass-ceramic with chemical and mechanical properties similar to those of glass. All designs and materials used fall within FDA rules. The electrical signal for the ultrasonic transducer was generated using a frequency power synthesizer (FPS 2540, PSI Systems, Austria). The ultrasonic field intensity and frequency were manually controlled, and the electrical power was set in the range of 1−3 W. A frequency of ≈2 MHz, corresponding to a sound

DOI: 10.1021/acs.analchem.9b01105
Anal. Chem. 2019, 91, 14231−14238

wavelength in the aqueous environment of ≈740 μm was applied, resulting in a distance of ≈370 μm between nodal planes. Two fundamentally different designs (see Figure 1a,b) were tested: in the first setup, the ultrasound standing wave field was set parallel to the propagation direction of the Raman laser. This allowed use of the lens of the Raman probe as a reflector for the acoustic resonator. In the second setup, the ultrasound wave field was oriented perpendicular to the propagation direction of the Raman laser. Thus, another Macor reflector was used to reflect the ultrasound waves. The second setup allows additional selectivity of the Raman measurements. The laser focus can be set either on or between the nodal planes depending on the frequency of the ultrasonic wave, allowing either the nodal or antinodal plane to be moved into the focus point of the excitation laser. Hence, the scattered photons will carry chemical-specific information on either the solid or liquid phase, enabling single-phase investigation in, for example, stirred suspensions. The prototype design and manufacturing for the perpendicular arrangement required sophisticated engineering approaches to ensure compliance with the geometry restrictions necessary for fitting to a D25 Ingold port. These spatial arrangement limitations necessitated a Raman probe with a focal length of 10 mm, which exceeds the focal length of commercial Raman probes for in-line measurements available in our lab by roughly a factor of 4. Consequently, a probe with a suitable focal length was fabricated using a stainless-steel tube and an antireflection-coated 8 mm diameter lens (Plano Convex Lens, Newport Corp.). Raman measurements in cyclohexane with the custom-made and the commercially available probe revealed identical Raman spectra in terms of band positions and higher signal intensity for the custom-made probe (see Figure S3). Therefore, the latter probe was used for in-line Raman measurements when employing the prototype that allows perpendicular arrangement of the Raman laser and ultrasonic wave propagation directions. A simplified setup was used for the initial test measurements, consisting of a commercial UV/vis cuvette with filling capacity of 3.5 mL (6030-OG, spectral range 360−2500 nm, Hellma GmbH, Germany) placed in a 3D-printed holder and fixed onto a manually operated xyz-stage (graduation: 10 μm; Thorlabs Inc., NJ). This setup allows the change in frequency of the ultrasonic waves to be mimicked by changing the position of the cuvette perpendicular to the Raman laser propagation direction. Line scans covering a distance of 1 mm along the propagation direction of the ultrasonic waves (y-direction) were performed with a step size of 50 μm.

Raman Measurements. Raman measurements employed an RXN1 Raman system (Kaiser Optical Systems Inc., an Endress+Hauser company, MI) equipped with a 785 nm laser and a low-frequency grating that allows access to the spectral region between 100 and 1890 cm^{-1} (Raman shift). Single spectra were recorded at maximum laser power (550 mW) using a charge-coupled device (CCD) detector. In order to balance signal-to-noise ratio (SNR) and measurement time, three spectra were accumulated with an integration time of 15 s each at 1 min measurement intervals. The settings used to acquire Raman spectra as well as parameters such as stirrer speed, vessel volume, and size of the resonator were kept constant for comparative purposes. Parameter settings for Raman measurements needed to be carefully adapted. Identical parameter settings were also used for measurements in a defined particle concentration range. Particle concentration and parameter settings were determined based on a balance between overall measurement time and SNR of single spectra. A strong increase in signal intensity was observed with active UPM. Hence, to stay within the dynamic range of the CCD, experimental parameters were chosen such that the Raman signal was just detectable at the highest particle concentration with conventional Raman spectroscopy while avoiding detector saturation for Raman measurements with active UPM. Each concentration was measured over three runs, where each measurement run consisted of acquiring a total of 42 spectra over 3 accumulation phases (ultrasound turned on) with 10 measurements each and 4 × 3 measurements with the ultrasound switched off. Between each run, the stirrer was set to maximum speed to counteract aggregation of particles and accumulation of analyte on the transducer surface.

Samples. Starch particles (ρ_{starch} = 1.5 g/cm^3, Merck KGaA, Germany) in an aqueous environment were chosen as the initial test system as starch is easy to handle, nontoxic, readily available, reasonably stable, and a good Raman scatterer. Additionally, the typical diameter of starch particles (roughly 10 μm) perfectly fits the size range (∼1 μm up to some 100 μm) accessible with the frequency of ∼2 MHz employed for particle trapping. Six starch concentrations ranging from 0.016 g/L to 0.5 g/L were investigated. Suspensions were prepared by weighing solid fractions of starch and adding 500 mL of deionized water before degassing the suspension in an ultrasound bath prior to Raman measurements. The band at 478 cm^{-1} was selected to monitor the effect of UPM on the Raman signal intensity; this is the most intense band in the spectral fingerprint region of starch and is attributed to C−C−C bend and C−O torsion vibrations.[17] Integration between 458 and 498 cm^{-1} with 2-point baseline subtraction allowed estimation of the signal enhancement achieved via ultrasound-enhanced Raman spectroscopy.

Similar experiments were performed using smaller-diameter (≈3 μm) poly(methyl methacrylate) (PMMA) particles (ρ_{PMMA} = 1.2 g/cm^3, Polysciences GmbH, Germany) in deionized water, mainly to study the effect of particle size on the particle trapping efficiency of the ultrasound field, as the primary acoustic radiation force strongly depends on this parameter ($F_z^{rad} \sim r^3$, see eq 1). PMMA also has several key properties such as (i) insolubility in water, (ii) good Raman scattering, and (iii) a narrow particle size distribution (3.36 μm ± 0.54 μm) in the lower micrometers range. The ν_s (C−O−C) vibration[18] at 818 cm^{-1} was selected as the PMMA marker band because it is one of the most intense bands in the spectral fingerprint of PMMA that experiences no spectral interference from water or the transducer material. Six PMMA concentrations ranging from 0.063 g/L to 2.0 g/L were investigated.

Data Processing. iC Raman software (version 4.1, Kaiser Optical Systems Inc., an Endress+Hauser company, MI) was used for data acquisition and integration of marker bands with a 2-point baseline. Spectra were cut to focus on defined spectral regions and/or baseline corrected using the asymmetric least-squares smoothing procedure of Eilers and Boelens[19] in Python 3.6.

DataLab (version 3.530, Epina GmbH, Pressbaum, Austria) and online calculators provided by Mathcrackers (https://mathcracker.com) were used for statistical evaluation of the ultrasound-enhanced Raman signal as a function of particle concentration.

DOI: 10.1021/acs.analchem.9b01105
Anal. Chem. 2019, 91, 14231−14238

RESULTS AND DISCUSSION

To evaluate the effect of UPM on the Raman signal intensity and level of detection, single spectra were first recorded in stirred suspensions of starch and PMMA of different concentrations without ultrasound; Raman spectra with active UPM in the acoustic resonator were then recorded. Visual inspection shows distinct differences between the images with and without UPM for both particle systems in the parallel arrangement (see Figure 2a). In the absence of an ultrasound field, particles are homogeneously distributed in the stirred suspension. Depending on the concentration, a particle occasionally passes in front of the probe such that interaction with the Raman laser is possible. The image of the PMMA suspension depicts the position of the laser focus in the lower half of the acoustic resonator (focal length of commercial probe: 2.4 mm). To exclude interference from the Macor bands in the spectral fingerprint of starch or PMMA particles, respectively, a greater distance is required between transducer and reflector, resulting in a weaker ultrasonic standing wave field. Balancing these two parameters (stability of the ultrasonic field vs Macor interference in the Raman spectra) resulted in selection of a distance of 2.5 mm between the lens (reflector) and transducer. As soon as the ultrasound is turned on, particles are actively caught in the standing wave field and concentrated in front of the Raman probe. For starch, 0.5 g/L was determined as the LOD of the in-line Raman probe as a weak Raman signal could typically be obtained. In contrast, a pronounced spectrum of the same particle concentration is observed with ultrasound enhancement (Figure 2b). The LOD for the in-line probe with UPM was as low as 0.016 g/L, i.e., a 30-fold improvement is demonstrated. The limitation here is mostly the time required to collect particles in the nodal planes: considering a stirred suspension with homogeneously distributed particles, the number of particles in close proximity to the ultrasound standing wave field is significantly reduced for lower concentrations at constant vessel volume (here, 500 mL). Therefore, a particle must travel a greater distance before being close enough to the standing wave field to be caught in the nodal planes compared to suspensions with higher particle concentrations. Hence, longer particle collection times would be needed for lower concentrations before similarly strong Raman signal intensities with the same parameters (laser power, integration time) could be detected. Consecutive periods with and without UPM indicate reproducible results with a significant signal increase for ultrasound-enhanced Raman spectra. As can be seen in Figure 2c, an increase in signal intensity of the integrated marker band from 0 to values in the range of 10^4 is observed as soon as the ultrasonic field is formed and particles are drawn into the nodal planes of the standing wave field. Similar observations were made for PMMA suspensions. However, PMMA solutions required more time than starch solutions for the Raman signal to plateau with active UPM. This observation can be linked to the radius and the material properties of the particles: starch and PMMA differ in particle size (starch ≈10 μm, PMMA ≈ 3 μm) and density (ρ_{starch} = 1.5 g/cm^3, ρ_{PMMA} = 1.2 g/cm^3 according to data sheets), both of which affect the primary axial radiation force (see eqs 1 and 2). The main impact is attributed to particle size ($F_z^{rad} \sim r^3$); thus, a significantly higher force (roughly 37× higher) is acting on the starch particles as they are dragged into the nodal planes, resulting in quicker collection of particles in front of the Raman probe.

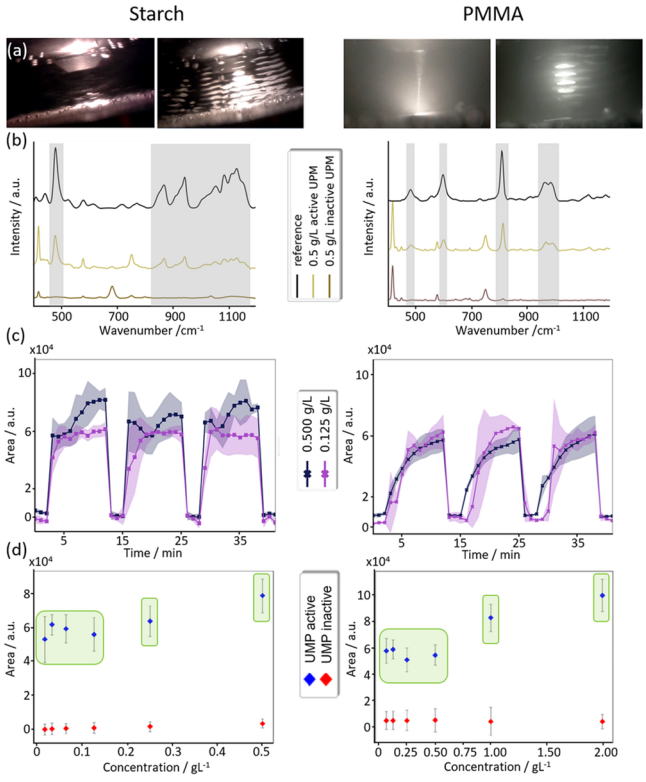

Figure 2. Two particle systems (starch and PMMA; primary difference is in particle size) were investigated with the parallel arrangement. (a) Video images with (right) and without (left) ultrasound particle manipulation (UPM), highlighting the effect of the primary axial radiation force on starch and PMMA particles, respectively. (b) Raman spectra of 0.5 g/L starch and PMMA extracted from phases with and without UPM are shown in comparison to a reference spectrum. Baseline-corrected spectra are normalized and offset for better comparison. (c) The integrated marker bands for two different concentrations of starch and PMMA as functions of time indicate different behaviors due to their different material properties (size, density). PMMA particles aggregate in the nodal planes more slowly than starch particles. Uncertainties are single standard deviations, indicated by the shaded, color-coded areas. (d) Six different concentrations of each particle system were investigated with (blue data points) and without (red data points) ultrasound. Statistically equal means/medians for ultrasound-active phases are framed in green.

As mentioned above, six concentrations each of starch and PMMA were investigated. The highest particle concentration for each system represents the achieved LOD of the employed Raman probe/spectrometer without particle manipulation. The Raman signal collected with active UPM shows considerable improvement in signal intensity; however, the linear correlation between signal intensity and analyte concentrations is lost to a certain extent, as depicted in Figure 2d. For conventional Raman spectroscopy, no starch- or PMMA-specific signal was detected for concentrations below 0.5 g/L starch or 2 g/L PMMA. Hence, no linear dependency for the signal intensity as a function of particle concentration can be shown. Depending on the material properties of the particle system and carrier medium, a certain concentration dependency of the Raman signal with ultrasound active phases is possible, although with a significantly reduced dynamic range compared to conventional Raman spectroscopy, by balancing particle collection time, stirrer speed, and photon collection

DOI: 10.1021/acs.analchem.9b01105
Anal. Chem. 2019, 91, 14231−14238

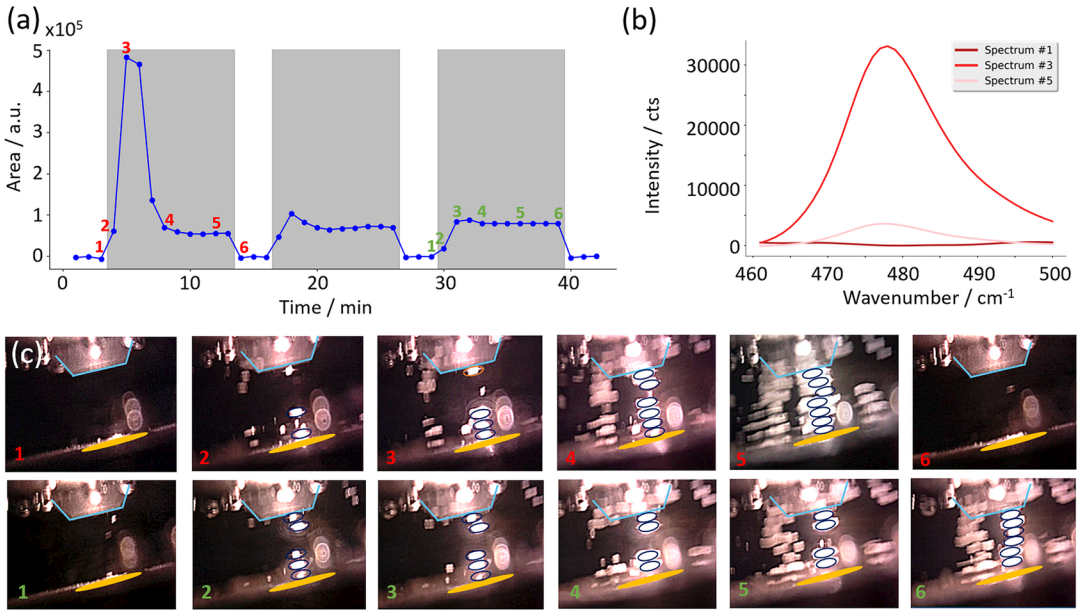

Figure 3. Ultrasound particle manipulation (UPM) of starch particles (0.031 g/L in a 500 mL vessel) using the parallel arrangement. (a) The intensity of the integrated starch marker band at 478 cm^{-1} (C−C−C bending, C−O torsion) increases significantly upon switching on the ultrasound (areas highlighted in gray) and drops to 0 as soon as the ultrasound is switched off. The first ultrasound-active phase (red numbers) differs from the following two phases. (b) As an example, the intensity of the starch marker band is shown for three different stages (1, 3, and 5) of the first ultrasound-active phase, as numbered in red in panel (a). (c) Video images of starch particles accumulating in the nodal planes of the ultrasound wave field with and without active UPM, corresponding to the numbered, color-coded events in panel (a), indicate different structures in the formation of the ultrasound standing wave field (images 2 and 3 colored in red and green) between the first and the following two ultrasound-active phases. The probe head is marked in light blue, the transducer is marked in yellow, and the particles in the nodal planes are marked in dark blue.

time on the CCD. On the basis of statistical tests (see Figures S1 and S2), means/medians of the four lowest concentrations of each particle system are considered to be equal, whereas there is not enough evidence to assume that the means/medians of 0.25 g/L and 0.5 g/L starch or 1 g/L and 2 g/L PMMA, respectively, are equal. The results of the statistical evaluation are summarized in Figure 2d, in which statistically equal means/medians are framed in green. Hence, for very low particle concentrations, only qualitative detection is possible.

In some cases, a strong signal increase was observed within the first few minutes of ultrasound activation. To shed some light on this behavior, the spatial arrangement of the particles in the nodal planes was studied in more detail using a commercial video camera (Pi camera operated by a Raspberry Pi 3) without a near-infrared (NIR) filter. Videos were recorded while the Raman measurements were taken, using the Raman laser as the light source for the camera images. Three consecutive measurements with alternating phases with and without UPM are shown as examples in Figure 3a for 0.031 g/L starch in an aqueous environment. Here, a strong increase of at least 7-fold is observed in the Raman signal (see Figure 3b depicting the starch marker band at different points in time along the first "ultrasound on" phase) during the first 2 min of the first "ultrasound on"-phase (highlighted in gray in Figure 3a); this phenomenon could not be repeated for the subsequent periods with active UPM. Video images at distinct time points during the measurement sequence were selected for the first and third ultrasound-active phase (Figure 3c). Color-coded numbers in the intensity plot (Figure 3a) mark the time points at which the respective video image was recorded. Images 4 and 5 of both ultrasound-active phases look very similar: starch particles are concentrated in front of the sensor, yielding two contrasting effects; with more particles agglomerating in front of the Raman probe, a higher Raman signal is achieved. However, at the same time, more particles are blocking the backscattered photons, attenuating the recorded Raman signal, although it is still significantly more intense than the measurements obtained without UPM (see Figure 3b). The two video images labeled 3 for both ultrasound-active phases are of particular interest: in both images, particles are concentrated in the focus point of the Raman probe. However, in the first ultrasound-active phase, fewer particles are blocking the backscattered photons in the upper area of the standing wave field (closer to the probe), which leads to a strong increase in the recorded Raman signal. In video image 4 of the first phase, particles are concentrated in all nodal planes between the transducer and the Raman probe, thus resulting in a lower Raman signal, as recorded for most of the other ultrasound-active phases.

Arrangement of the laser and ultrasound wave propagation directions perpendicular to one another (see Figure 1b) allows not only increased signal sensitivity but also additional selectivity of in-line Raman measurements of suspensions. In the perpendicular arrangement, particles in the nodal planes are selectively moved in or out of the laser focus by changing the frequency of the ultrasonic wave, allowing selective investigation of either the liquid or the solid phase. The design of this arrangement to fit a D25 Ingold port requires a complex, refined design of the probe add-on; thus, limitations regarding strength and stability of the ultrasound standing wave field must be considered in the first iteration of this prototype. Before realizing this complex design, test measurements were performed using an experimental setup consisting of a UV/vis cuvette filled with 6 g/L PMMA in water on a

DOI: 10.1021/acs.analchem.9b01105
Anal. Chem. 2019, 91, 14231−14238

manually operated xyz-stage. Two piezoelectric elements were glued to two opposing sides of the cuvette to act as a transducer and reflector, respectively, thus forming an acoustic resonator within the cuvette. The experimental arrangement is shown in Figure 4a. In the final prototype, the particles

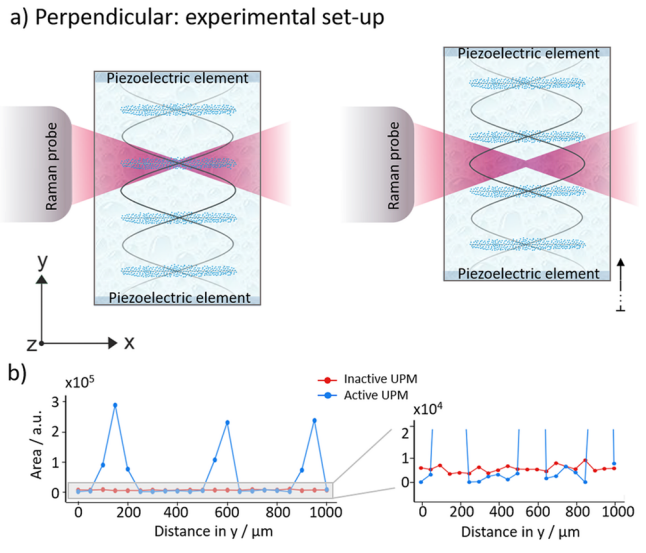

Figure 4. Experimental setup for test measurements with the Raman laser and ultrasonic wave propagation directions arranged perpendicularly. (a) Two piezoelectric elements acting as transducer and reflector are placed on opposite sides of a glass UV/vis cuvette mounted on an *xyz*-stage. The PMMA particles agglomerated in the nodal planes of the ultrasonic standing wave field are moved in and out of the laser focus by manually moving the cuvette in the *y*-direction. (b) Line scans along the *y*-axis with a step size of 50 μm with (blue) and without (red) active ultrasound particle manipulation (UPM). The Raman signal collected from particles in the nodal planes is significantly higher compared to the signal collected between nodal planes. Enlargement of the baseline shows that the PMMA-specific signal is higher in the stirred suspension without UPM compared to the Raman signal collected between nodal planes with UPM.

accumulated in the nodal planes are moved in and out of the laser focus by changing the frequency of the ultrasonic waves. In the preliminary setup, the cuvette fixed on the *xyz*-stage was moved manually in the *y*-direction (perpendicular to the Raman laser direction but parallel to the ultrasonic wave propagation) to mimic the change in the frequency of the ultrasonic waves and to investigate how much selectivity can effectively be gained with this arrangement. Line scans across nodal and antinodal planes measured consecutively with and without active UPM, respectively, are shown in Figure 4b (additional data shown in Figure S4). The intensity distribution of the integrated PMMA marker band [ν_s(C−O−C) vibration at 818 cm^{-1}] along the 1 mm scanned area clearly illustrates the presence of three nodal planes, indicated by the significantly higher signal intensity in these areas. Comparison of the band areas of the nodal planes with the band areas of the stirred suspension without UPM indicates a 42-fold improvement of the signal. Enlargement of the baseline area in Figure 4b shows that the PMMA-specific signal is higher in stirred suspension without active UPM compared to the signal taken in areas between the nodal planes under active particle manipulation. A significant portion of the particles in the suspension are drawn into the nodal planes, leaving few particles in the areas between the planes; hence, a significantly lower or no PMMA-specific Raman signal is expected in these areas, as is clearly reflected in the line scans (Figure 4b, right-hand side). These line scans indicate that the nodal planes with agglomerated particles have a width of 100 to 150 μm and that the distance between the maximum of each nodal plane is 300 μm ± 50 μm, which correlates well with the expected distance based on the set frequency of the ultrasonic waves. Note that during measurements, rearrangement of particles in nodal planes and slight shifts of nodal planes as a consequence thereof were observed. On the one hand, this can be the result of temperature changes in the suspension due to energy input of the ultrasonic waves and a certain heat impact of the magnetic stirrer. For example, if the temperature of the medium increases from 20 to 25 °C, the temperature dependency of the speed of sound in water[20] results in a change of the ultrasonic wavelength of $\Delta\lambda$ = 7 μm for a 2 MHz wave. This shows that system parameters must be well controlled to allow accurate measurements between and on nodal planes for the perpendicular arrangement. Considering the small vessel volume of 3.5 mL of the UV/vis cuvette, the heat impact is significantly higher here compared to the heat impact in a 500 mL beaker, and the heat impact should be insignificant in temperature-controlled vessels. On the other hand, constant particle rearrangement in the nodal planes due to the transverse primary radiation force F_{xy}^{rad} and the secondary radiation force F_{xyz}^{i} acting on the particles has an impact on the form of the aggregates in the nodal planes. Nevertheless, a significant gain in selectivity for in-line Raman measurements was observed. Therefore, the design of a second prototype with perpendicular propagation of the Raman laser and ultrasound wave was realized.

As for experiments with the parallel arrangement, starch in an aqueous environment was chosen as a test system for the perpendicular arrangement. Again, signal intensity was quantified by integration of the starch-specific band at 478 cm^{-1} with a 2-point baseline between the integration limits of 458 and 498 cm^{-1}. As can be seen in Figure 5, the value of the integrated starch band for measurements on the nodal plane is the same order of magnitude (10^5) as was temporarily observed in the strong signal increase for the parallel arrangement (as shown in Figure 3a). In contrast to the parallel arrangement, the signal intensity in the perpendicular arrangement can be kept at this high level during active UPM and drops to zero as soon as the ultrasound is switched off. It is also noticeable that particles are caught within the nodal planes within seconds of switching the ultrasonic field on (gray area in Figure 5c), resulting in a detectable signal increase within the first minute (spectrum #2 in Figure 5a) of the ultrasound active-phase highlighted in gray in Figure 5c. Video images recorded simultaneously with the Raman spectra also depict this rapid accumulation of particles in the nodal planes (Figure 5b). As previously mentioned, in addition to increased signal intensity, the selectivity of the in-line Raman probe significantly increases in the perpendicular arrangement. In Figure 6, starch particles are selectively moved into or out of the probe's focus depending on the frequency f_1 or f_2 of the ultrasonic waves ($\Delta f \approx$ 30 kHz). On the basis of theoretical considerations, a change in frequency of 30 kHz induces a shift of the agglomerated particles in the nodal planes of ≈14 μm. The custom-made probe in combination with the 785 nm Raman laser allows a laser spot size of ≈3 μm and a spatial resolution of ≈1.4 μm. Hence, a shift of the

DOI: 10.1021/acs.analchem.9b01105
Anal. Chem. 2019, 91, 14231−14238

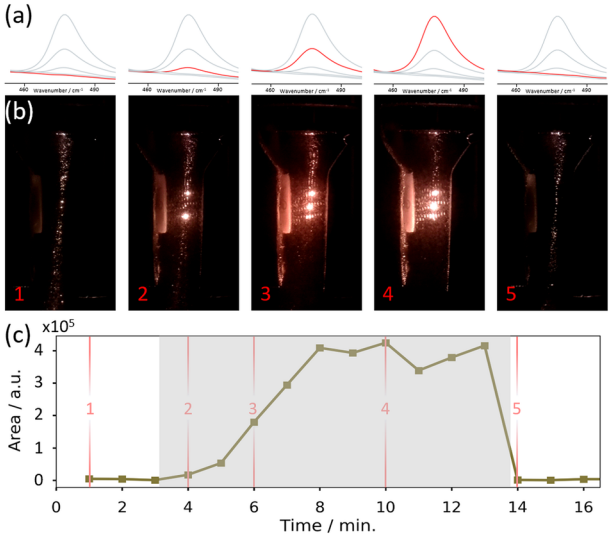

Figure 5. Ultrasound particle manipulation (UPM) of starch particles using the perpendicular arrangement. (a) The starch marker band at 478 cm^{-1} (C−C−C bending, C−O torsion) is clearly visible during UPM (spectra in the middle), while a flat line is recorded upon switching the ultrasound off (spectra on the left and right edge). (b) Video images of the acoustic resonator in front of the Raman probe with (images 2−4) and without (images 1 and 5) active UPM, corresponding to the numbered events in panel (c). (c) The starch marker band area increases significantly upon switching the ultrasound on (highlighted in gray), directly proportional to the intensity of scattered laser light in the video images, and drops upon switching the ultrasound off.

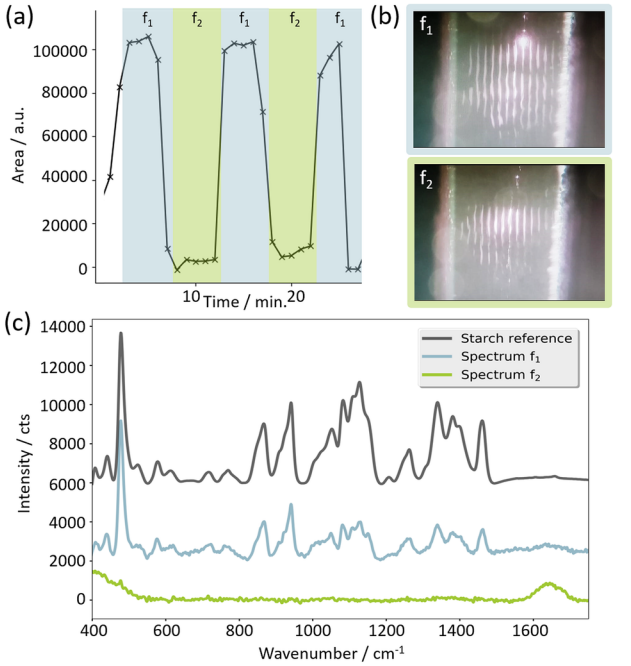

Figure 6. Starch particles are moved into and out of the laser focus point by changing the frequency of the ultrasonic waves in the kHz range. (a) The intensity of the integrated starch band [gray in panel (c)] changes significantly depending on the ultrasound frequency. (b) At f_1, the laser focus is on a nodal plane; accumulated starch particles are indicated by the bright point in the upper part of the image due to intense scattering effects. This intense scattering of the Raman laser is not observed when the laser is focused between nodal planes (f_2). (c) The selectivity based on the selected ultrasound frequency is reflected in the recorded Raman spectra, which carry starch-specific information for f_1 and lack the characteristic starch spectral fingerprint for f_2. Spectra are baseline-corrected, scaled (1/40 of the intensity of the reference spectrum), and offset for better comparison.

agglomerated particles of 14 μm is sufficient to selectively measure the liquid phase between nodal planes. Additionally, the transverse primary radiation force F_{xy}^{rad} had an observable impact on the 3D arrangement of particles in the ultrasonic standing wave field. Changing the ultrasonic frequency from f_1 to f_2 led to a rearrangement of particles in the z-dimension, resulting in particles temporarily falling out of the laser focus point. Note that this effect is reversible (Figure 6a). The selectivity induced by the change in frequency is reflected in the information carried by the backscattered Raman photons: spectra recorded at f_1 (laser focus on nodal plane with accumulated starch particles) show the characteristic starch spectral fingerprint, which correlates well with the reference spectrum of starch powder (see Figure 6c), whereas no starch signal is detectable in the spectra recorded at f_2. The decrease and increase of the integrated starch marker band based on the frequency of the ultrasonic waves is demonstrated in Figure 6a. Video images at f_1 and f_2 (Figure 6b) highlight the laser focus on the line at f_1, as indicated by the intense scatter effect on concentrated starch particles, whereas no direct light scattering on starch particles is observed for f_2.

CONCLUSION

This work demonstrates the combination of in-line Raman spectroscopy with ultrasound particle manipulation. Two different arrangements of the laser propagation direction and ultrasonic wave propagation are realized. Increased sensitivity and selectivity are demonstrated in measurements of starch and PMMA suspensions at six different concentrations each. The parallel arrangement exhibited an ~30-fold improvement in the limit of detection of the recorded Raman spectra. Whereas the values of the integrated starch marker bands were typically on the scale of 10^4, the perpendicular arrangement promises even greater signal improvement (by an additional factor of 10). To achieve optimal signal sensitivity in Raman spectroscopy, lenses with a high numerical aperture are used. Usually, short focal lengths (for constant lens diameter) are preferred. Hence, future developments in the parallel arrangement will investigate better adaptation of the acoustic resonator's geometry and the Raman probe's focal length. The efficiency of the parallel arrangement can be substantially improved by designing a more compact system, for instance with a shorter-focal-length lens. Such a design would have two advantages: (i) the distance between transducer and reflector can be reduced, leading to a stronger and more stable standing wave field and hence more efficient particle manipulation. (ii) If the focus point is directly in front of the Raman probe (focal length of similar scale as the distance between nodal planes) then the negative impact of particles accumulating between the lens and the focus point and the resulting weakened recorded Raman signal can be circumvented.

The perpendicular arrangement additionally offers selective investigation of either the liquid or the solid phase of suspensions. However, further improvements are needed, such as enhanced stability of the ultrasonic standing wave field, e.g., by using a different amplifier or by increasing the size of the transducer surface. Also, until now, the frequency of the ultrasonic waves has been manually controlled for both arrangements. Hence, automated frequency regulation, allow-

DOI: 10.1021/acs.analchem.9b01105
Anal. Chem. 2019, 91, 14231−14238

ing particles to be caught in the nodal planes without manual regulation, is desired to allow stable in-line measurements.

Having now introduced the general working principles of ultrasound-enhanced in-line Raman sensing, future work will concentrate on the investigation of products, byproducts, or impurities in process analytical chemistry. Envisioned applications include crystallization processes, where the crystallization type can be determined by focusing on the crystals accumulating in the nodal planes and the composition of liquid phases can be accessed by changing the frequency of the ultrasonic waves in the acoustic resonator, allowing the laser to be focused between nodal planes. Other applications involve analysis of oil in water, wastewater treatment, and others where gains in sensitivity and/or selectivity will allow optimized, accurate, real-time process monitoring and control.

■ ASSOCIATED CONTENT

Supporting Information

The Supporting Information is available free of charge on the ACS Publications website at DOI: 10.1021/acs.analchem.9b01105.

Details on statistical evaluation of ultrasound-enhanced Raman signal as a function of particle concentration, comparison of cyclohexane Raman spectra recorded with commercial and custom-made probe, and line scan parallel to the ultrasonic wave propagation direction in the cuvette (PDF)

■ AUTHOR INFORMATION

Corresponding Author

*Address:, Institute of Chemical Technologies and Analytics, Vienna University of Technology (TU Wien), Getreidemarkt 9/164, 1060 Vienna, Austria. E-mail: bernhard.lendl@tuwien.ac.at.

ORCID

Karin Wieland: 0000-0002-4535-5679

Christoph Gasser: 0000-0002-6329-2560

Author Contributions

All authors contributed to the writing of this manuscript. All authors have given approval to the final version of the manuscript.

Notes

The authors declare no competing financial interest.

■ ACKNOWLEDGMENTS

The authors acknowledge financial support through the COMET Centre CHASE (project No 868615), which is funded within the framework of COMET − Competence Centers for Excellent Technologies by BMVIT, BMDW, the Federal Provinces of Upper Austria and Vienna. The COMET programme is run by the Austrian Research Promotion Agency (FFG). This work was also supported by Kaiser Optical Systems, Inc., an Endress+Hauser company, within the Center of Excellence "Ultrasound Enhanced In-Line Raman Spectroscopy." S.R. received funding from the European Union's Horizon 2020 research and innovation program under Grant 731778.

■ REFERENCES

(1) De Beer, T. R. M.; Baeyens, W. R. G.; Ouyang, J.; Vervaet, C.; Remon, J. P. *Analyst* **2006**, *131*, 1137−1144.

(2) Li, Y.; Anderson, C. A.; Drennen, J. K.; Airiau, C.; Igne, B. *Anal. Chem.* **2018**, *90*, 8436−8444.

(3) Matthiae, M.; Zhu, X.; Marie, R.; Kristensen, A. *Analyst* **2019**, *144*, 602−610.

(4) Hippler, M. *Anal. Chem.* **2015**, *87*, 7803−7809.

(5) Zhang, X.; Tan, Q.-H.; Wu, J.; Shi, W.; Tan, P.-H. *Nanoscale* **2016**, *8*, 6435−6450.

(6) Wang, Q.; Li, Z.; Ma, Z.; Liang, L. *Sens. Actuators, B* **2014**, *202*, 426−432.

(7) Soares, F. L. F.; Carneiro, R. L. *Spectrochim. Acta, Part A* **2017**, *180*, 1−8.

(8) Csontos, I.; Pataki, H.; Farkas, A.; Bata, H.; Vajna, B.; Nagy, Z. K.; Keglevich, G.; Marosi, G. J. *Org. Process Res. Dev.* **2015**, *19*, 189−195.

(9) Koch, C.; Brandstetter, M.; Wechselberger, P.; Lorantfy, B.; Plata, M. R.; Radel, S.; Herwig, C.; Lendl, B. *Anal. Chem.* **2015**, *87*, 2314−2320.

(10) Radel, S.; Schnöller, J.; Dominguez, A.; Lendl, B.; Gröschl, M.; Benes, E. *Elektrotechnik & Informationstechnik* **2008**, *125*, 82−85.

(11) Ruedas-Rama, M. J.; Domınguez-Vidal, A.; Radel, S.; Lendl, B. *Anal. Chem.* **2007**, *79*, 7853−7857.

(12) Bruus, H. *Lab Chip* **2012**, *12*, 1014−1021.

(13) Gröschl, M. *Acta Acust* **1998**, *84*, 432−447.

(14) Gröschl, M. *Acta Acust* **1998**, *84*, 632−642.

(15) Benes, E.; Groschl, M.; Nowotny, H.; Trampler, F.; Keijzer, T.; Bohm, H.; Radel, S.; Gherardini, L.; Hawkes, J.J.; Konig, R.; Delouvroy, C.. *Proc. IEEE Ultrason. Symp.* **2001**, 649−659.

(16) Settnes, M.; Bruus, H. *Phys. Rev. E* **2012**, *85*, 1−12.

(17) Almeida, M. R.; Alves, R. S.; Nascimbem, L. B. L. R.; Stephani, R.; Poppi, R. J.; De Oliveira, L. F. C. *Anal. Bioanal. Chem.* **2010**, *397*, 2693−2701.

(18) Willis, H. A.; Zichy, V. J. I.; Hendra, P. J. *Polymer* **1969**, *10*, 737−746.

(19) Eilers, P. H. C.; Boelens, H. F. M. Baseline Correction with Asymmetric Least Squares Smoothing. **2005** https://zanran_storage.s3.amazonaws.com/www.science.uva.nl/ContentPages/443199618.pdf.

(20) Greenspan, M.; Tschiegg, C. E. *J. Res. Natl. Inst. Stand. Technol.* **1957**, *59*, 249−254.

DOI: 10.1021/acs.analchem.9b01105
Anal. Chem. 2019, 91, 14231−14238